Measurements of $\psi(3686) \to K^-\Lambda\bar{\Xi}^+ + \mathrm{c.c.}$ and $\psi(3686) \to \gamma K^-\Lambda\bar{\Xi}^+ + \mathrm{c.c.}$

M. Ablikim,[1] M. N. Achasov,[9,a] X. C. Ai,[1] O. Albayrak,[5] M. Albrecht,[4] D. J. Ambrose,[44] A. Amoroso,[48a,48c] F. F. An,[1] Q. An,[45] J. Z. Bai,[1] R. Baldini Ferroli,[20a] Y. Ban,[31] D. W. Bennett,[19] J. V. Bennett,[5] M. Bertani,[20a] D. Bettoni,[21a] J. M. Bian,[43] F. Bianchi,[48a,48c] E. Boger,[23,h] O. Bondarenko,[25] I. Boyko,[23] R. A. Briere,[5] H. Cai,[50] X. Cai,[1] O. Cakir,[40a,b] A. Calcaterra,[20a] G. F. Cao,[1] S. A. Cetin,[40b] J. F. Chang,[1] G. Chelkov,[23,c] G. Chen,[1] H. S. Chen,[1] H. Y. Chen,[2] J. C. Chen,[1] M. L. Chen,[1] S. J. Chen,[29] X. Chen,[1] X. R. Chen,[26] Y. B. Chen,[1] H. P. Cheng,[17] X. K. Chu,[31] G. Cibinetto,[21a] D. Cronin-Hennessy,[43] H. L. Dai,[1] J. P. Dai,[34] A. Dbeyssi,[14] D. Dedovich,[23] Z. Y. Deng,[1] A. Denig,[22] I. Denysenko,[23] M. Destefanis,[48a,48c] F. De Mori,[48a,48c] Y. Ding,[27] C. Dong,[30] J. Dong,[1] L. Y. Dong,[1] M. Y. Dong,[1] S. X. Du,[52] P. F. Duan,[1] J. Z. Fan,[39] J. Fang,[1] S. S. Fang,[1] X. Fang,[45] Y. Fang,[1] L. Fava,[48b,48c] F. Feldbauer,[22] G. Felici,[20a] C. Q. Feng,[45] E. Fioravanti,[21a] M. Fritsch,[14,22] C. D. Fu,[1] Q. Gao,[1] X. Y. Gao,[2] Y. Gao,[39] Z. Gao,[45] I. Garzia,[21a] C. Geng,[45] K. Goetzen,[10] W. X. Gong,[1] W. Gradl,[22] M. Greco,[48a,48c] M. H. Gu,[1] Y. T. Gu,[12] Y. H. Guan,[1] A. Q. Guo,[1] L. B. Guo,[28] Y. Guo,[1] Y. P. Guo,[22] Z. Haddadi,[25] A. Hafner,[22] S. Han,[50] Y. L. Han,[1] X. Q. Hao,[15] F. A. Harris,[42] K. L. He,[1] Z. Y. He,[30] T. Held,[4] Y. K. Heng,[1] Z. L. Hou,[1] C. Hu,[28] H. M. Hu,[1] J. F. Hu,[48a,48c] T. Hu,[1] Y. Hu,[1] G. M. Huang,[6] G. S. Huang,[45] H. P. Huang,[50] J. S. Huang,[15] X. T. Huang,[33] Y. Huang,[29] T. Hussain,[47] Q. Ji,[1] Q. P. Ji,[30] X. B. Ji,[1] X. L. Ji,[1] L. L. Jiang,[1] L. W. Jiang,[50] X. S. Jiang,[1] J. B. Jiao,[33] Z. Jiao,[17] D. P. Jin,[1] S. Jin,[1] T. Johansson,[49] A. Julin,[43] N. Kalantar-Nayestanaki,[25] X. L. Kang,[1] X. S. Kang,[30] M. Kavatsyuk,[25] B. C. Ke,[5] R. Kliemt,[14] B. Kloss,[22] O. B. Kolcu,[40b,d] B. Kopf,[4] M. Kornicer,[42] W. Kühn,[24] A. Kupsc,[49] W. Lai,[1] J. S. Lange,[24] M. Lara,[19] P. Larin,[14] C. Leng,[48c] C. H. Li,[1] Cheng Li,[45] D. M. Li,[52] F. Li,[1] G. Li,[1] H. B. Li,[1] J. C. Li,[1] Jin Li,[32] K. Li,[13] K. Li,[33] Lei Li,[3] P. R. Li,[41] T. Li,[33] W. D. Li,[1] W. G. Li,[1] X. L. Li,[33] X. M. Li,[12] X. N. Li,[1] X. Q. Li,[30] Z. B. Li,[38] H. Liang,[45] Y. F. Liang,[36] Y. T. Liang,[24] G. R. Liao,[11] D. X. Lin,[14] B. J. Liu,[1] C. X. Liu,[1] F. H. Liu,[35] Fang Liu,[1] Feng Liu,[6] H. B. Liu,[12] H. H. Liu,[1] H. H. Liu,[16] H. M. Liu,[1] J. Liu,[1] J. P. Liu,[50] J. Y. Liu,[1] K. Liu,[39] K. Y. Liu,[27] L. D. Liu,[31] P. L. Liu,[1] Q. Liu,[41] S. B. Liu,[45] X. Liu,[26] X. X. Liu,[41] Y. B. Liu,[30] Z. A. Liu,[1] Zhiqiang Liu,[1] Zhiqing Liu,[22] H. Loehner,[25] X. C. Lou,[1,e] H. J. Lu,[17] J. G. Lu,[1] R. Q. Lu,[18] Y. Lu,[1] Y. P. Lu,[1] C. L. Luo,[28] M. X. Luo,[51] T. Luo,[42] X. L. Luo,[1] M. Lv,[1] X. R. Lyu,[41] F. C. Ma,[27] H. L. Ma,[1] L. L. Ma,[33] Q. M. Ma,[1] S. Ma,[1] T. Ma,[1] X. N. Ma,[30] X. Y. Ma,[1] F. E. Maas,[14] M. Maggiora,[48a,48c] Q. A. Malik,[47] Y. J. Mao,[31] Z. P. Mao,[1] S. Marcello,[48a,48c] J. G. Messchendorp,[25] J. Min,[1] T. J. Min,[1] R. E. Mitchell,[19] X. H. Mo,[1] Y. J. Mo,[6] C. Morales Morales,[14] K. Moriya,[19] N. Yu. Muchnoi,[9,a] H. Muramatsu,[43] Y. Nefedov,[23] F. Nerling,[14] I. B. Nikolaev,[9,a] Z. Ning,[1] S. Nisar,[8] S. L. Niu,[1] X. Y. Niu,[1] S. L. Olsen,[32] Q. Ouyang,[1] S. Pacetti,[20b] P. Patteri,[20a] M. Pelizaeus,[4] H. P. Peng,[45] K. Peters,[10] J. Pettersson,[49] J. L. Ping,[28] R. G. Ping,[1] R. Poling,[43] Y. N. Pu,[18] M. Qi,[29] S. Qian,[1] C. F. Qiao,[41] L. Q. Qin,[33] N. Qin,[50] X. S. Qin,[1] Y. Qin,[31] Z. H. Qin,[1] J. F. Qiu,[1] K. H. Rashid,[47] C. F. Redmer,[22] H. L. Ren,[18] M. Ripka,[22] G. Rong,[1] X. D. Ruan,[12] V. Santoro,[21a] A. Sarantsev,[23,f] M. Savrié,[21b] K. Schoenning,[49] S. Schumann,[22] W. Shan,[31] M. Shao,[45] C. P. Shen,[2] P. X. Shen,[30] X. Y. Shen,[1] H. Y. Sheng,[1] W. M. Song,[1] X. Y. Song,[1] S. Sosio,[48a,48c] S. Spataro,[48a,48c] G. X. Sun,[1] J. F. Sun,[15] S. S. Sun,[1] Y. J. Sun,[45] Y. Z. Sun,[1] Z. J. Sun,[1] Z. T. Sun,[19] C. J. Tang,[36] X. Tang,[1] I. Tapan,[40c] E. H. Thorndike,[44] M. Tiemens,[25] D. Toth,[43] M. Ullrich,[24] I. Uman,[40b] G. S. Varner,[42] B. Wang,[30] B. L. Wang,[41] D. Wang,[31] D. Y. Wang,[31] K. Wang,[1] L. L. Wang,[1] L. S. Wang,[1] M. Wang,[33] P. Wang,[1] P. L. Wang,[1] Q. J. Wang,[1] S. G. Wang,[31] W. Wang,[1] X. F. Wang,[39] Y. D. Wang,[20a] Y. F. Wang,[1] Y. Q. Wang,[22] Z. Wang,[1] Z. G. Wang,[1] Z. H. Wang,[45] Z. Y. Wang,[1] T. Weber,[22] D. H. Wei,[11] J. B. Wei,[31] P. Weidenkaff,[22] S. P. Wen,[1] U. Wiedner,[4] M. Wolke,[49] L. H. Wu,[1] Z. Wu,[1] L. G. Xia,[39] Y. Xia,[18] D. Xiao,[1] Z. J. Xiao,[28] Y. G. Xie,[1] Q. L. Xiu,[1] G. F. Xu,[1] L. Xu,[1] Q. J. Xu,[13] Q. N. Xu,[41] X. P. Xu,[37] L. Yan,[45] W. B. Yan,[45] W. C. Yan,[45] Y. H. Yan,[18] H. X. Yang,[1] L. Yang,[50] Y. Yang,[6] Y. X. Yang,[11] H. Ye,[1] M. Ye,[1] M. H. Ye,[7] J. H. Yin,[1] B. X. Yu,[1] C. X. Yu,[30] H. W. Yu,[31] J. S. Yu,[26] C. Z. Yuan,[1] W. L. Yuan,[29] Y. Yuan,[1] A. Yuncu,[40b,g] A. A. Zafar,[47] A. Zallo,[20a] Y. Zeng,[18] B. X. Zhang,[1] B. Y. Zhang,[1] C. Zhang,[29] C. C. Zhang,[1] D. H. Zhang,[1] H. H. Zhang,[38] H. Y. Zhang,[1] J. J. Zhang,[1] J. L. Zhang,[1] J. Q. Zhang,[1] J. W. Zhang,[1] J. Y. Zhang,[1] J. Z. Zhang,[1] K. Zhang,[1] L. Zhang,[1] S. H. Zhang,[1] X. Y. Zhang,[33] Y. Zhang,[1] Y. H. Zhang,[1] Y. T. Zhang,[45] Z. H. Zhang,[6] Z. P. Zhang,[45] Z. Y. Zhang,[50] G. Zhao,[1] H. S. Zhao,[1] J. W. Zhao,[1] J. Y. Zhao,[1] J. Z. Zhao,[1] Lei Zhao,[45] Ling Zhao,[1] M. G. Zhao,[30] Q. Zhao,[1] Q. W. Zhao,[1] S. J. Zhao,[52] T. C. Zhao,[1] Y. B. Zhao,[1] Z. G. Zhao,[45] A. Zhemchugov,[23,h] B. Zheng,[46] J. P. Zheng,[1] W. J. Zheng,[33] Y. H. Zheng,[41] B. Zhong,[28] L. Zhou,[1] Li Zhou,[30] X. Zhou,[50] X. K. Zhou,[45] X. R. Zhou,[45] X. Y. Zhou,[1] K. Zhu,[1] K. J. Zhu,[1] S. Zhu,[1] X. L. Zhu,[39] Y. C. Zhu,[45] Y. S. Zhu,[1] Z. A. Zhu,[1] J. Zhuang,[1] L. Zotti,[48a,48c] B. S. Zou,[1] and J. H. Zou[1]

(BESIII Collaboration)

[1]*Institute of High Energy Physics, Beijing 100049, People's Republic of China*
[2]*Beihang University, Beijing 100191, People's Republic of China*
[3]*Beijing Institute of Petrochemical Technology, Beijing 102617, People's Republic of China*
[4]*Bochum Ruhr-University, D-44780 Bochum, Germany*
[5]*Carnegie Mellon University, Pittsburgh, Pennsylvania 15213, USA*
[6]*Central China Normal University, Wuhan 430079, People's Republic of China*

[7]*China Center of Advanced Science and Technology, Beijing 100190, People's Republic of China*
[8]*COMSATS Institute of Information Technology, Lahore, Defence Road, Off Raiwind Road, 54000 Lahore, Pakistan*
[9]*G.I. Budker Institute of Nuclear Physics SB RAS (BINP), Novosibirsk 630090, Russia*
[10]*GSI Helmholtzcentre for Heavy Ion Research GmbH, D-64291 Darmstadt, Germany*
[11]*Guangxi Normal University, Guilin 541004, People's Republic of China*
[12]*GuangXi University, Nanning 530004, People's Republic of China*
[13]*Hangzhou Normal University, Hangzhou 310036, People's Republic of China*
[14]*Helmholtz Institute Mainz, Johann-Joachim-Becher-Weg 45, D-55099 Mainz, Germany*
[15]*Henan Normal University, Xinxiang 453007, People's Republic of China*
[16]*Henan University of Science and Technology, Luoyang 471003, People's Republic of China*
[17]*Huangshan College, Huangshan 245000, People's Republic of China*
[18]*Hunan University, Changsha 410082, People's Republic of China*
[19]*Indiana University, Bloomington, Indiana 47405, USA*
[20a]*INFN Laboratori Nazionali di Frascati, I-00044 Frascati, Italy*
[20b]*INFN and University of Perugia, I-06100 Perugia, Italy*
[21a]*INFN Sezione di Ferrara, I-44122 Ferrara, Italy*
[21b]*University of Ferrara, I-44122 Ferrara, Italy*
[22]*Johannes Gutenberg University of Mainz, Johann-Joachim-Becher-Weg 45, D-55099 Mainz, Germany*
[23]*Joint Institute for Nuclear Research, 141980 Dubna, Moscow region, Russia*
[24]*Justus Liebig University Giessen, II. Physikalisches Institut, Heinrich-Buff-Ring 16, D-35392 Giessen, Germany*
[25]*KVI-CART, University of Groningen, NL-9747 AA Groningen, Netherlands*
[26]*Lanzhou University, Lanzhou 730000, People's Republic of China*
[27]*Liaoning University, Shenyang 110036, People's Republic of China*
[28]*Nanjing Normal University, Nanjing 210023, People's Republic of China*
[29]*Nanjing University, Nanjing 210093, People's Republic of China*
[30]*Nankai University, Tianjin 300071, People's Republic of China*
[31]*Peking University, Beijing 100871, People's Republic of China*
[32]*Seoul National University, Seoul 151-747, Korea*
[33]*Shandong University, Jinan 250100, People's Republic of China*
[34]*Shanghai Jiao Tong University, Shanghai 200240, People's Republic of China*
[35]*Shanxi University, Taiyuan 030006, People's Republic of China*
[36]*Sichuan University, Chengdu 610064, People's Republic of China*
[37]*Soochow University, Suzhou 215006, People's Republic of China*
[38]*Sun Yat-Sen University, Guangzhou 510275, People's Republic of China*
[39]*Tsinghua University, Beijing 100084, People's Republic of China*
[40a]*Istanbul Aydin University, 34295 Sefakoy, Istanbul, Turkey*
[40b]*Dogus University, 34722 Istanbul, Turkey*
[40c]*Uludag University, 16059 Bursa, Turkey*
[41]*University of Chinese Academy of Sciences, Beijing 100049, People's Republic of China*
[42]*University of Hawaii, Honolulu, Hawaii 96822, USA*
[43]*University of Minnesota, Minneapolis, Minnesota 55455, USA*
[44]*University of Rochester, Rochester, New York 14627, USA*
[45]*University of Science and Technology of China, Hefei 230026, People's Republic of China*
[46]*University of South China, Hengyang 421001, People's Republic of China*
[47]*University of the Punjab, Lahore 54590, Pakistan*
[48a]*University of Turin, I-10125 Turin, Italy*
[48b]*University of Eastern Piedmont, I-15121 Alessandria, Italy*

[a]Also at the Novosibirsk State University, Novosibirsk 630090, Russia.
[b]Also at Ankara University, 06100 Tandogan, Ankara, Turkey.
[c]Also at the Moscow Institute of Physics and Technology, Moscow 141700, Russia and the Functional Electronics Laboratory, Tomsk State University, Tomsk 634050, Russia.
[d]Present address: Istanbul Arel University, 34295 Istanbul, Turkey.
[e]Also at University of Texas at Dallas, Richardson, Texas 75083, USA.
[f]Also at the NRC "Kurchatov Institute," PNPI, 188300 Gatchina, Russia.
[g]Also at Bogazici University, 34342 Istanbul, Turkey.
[h]Also at the Moscow Institute of Physics and Technology, Moscow 141700, Russia.

[48c]INFN, I-10125 Turin, Italy
[49]Uppsala University, Box 516, SE-75120 Uppsala, Sweden
[50]Wuhan University, Wuhan 430072, People's Republic of China
[51]Zhejiang University, Hangzhou 310027, People's Republic of China
[52]Zhengzhou University, Zhengzhou 450001, People's Republic of China
(Received 9 April 2015; published 22 May 2015)

Using a sample of $1.06 \times 10^8 \psi(3686)$ events produced in e^+e^- collisions at $\sqrt{s} = 3.686$ GeV and collected with the BESIII detector at the BEPCII collider, we present studies of the decays $\psi(3686) \to K^-\Lambda\bar{\Xi}^+ + \text{c.c.}$ and $\psi(3686) \to \gamma K^-\Lambda\bar{\Xi}^+ + \text{c.c.}$. We observe two hyperons, $\Xi(1690)^-$ and $\Xi(1820)^-$, in the $K^-\Lambda$ invariant mass distribution in the decay $\psi(3686) \to K^-\Lambda\bar{\Xi}^+ + \text{c.c.}$ with significances of 4.9σ and 6.2σ, respectively. The branching fractions of $\psi(3686) \to K^-\Lambda\bar{\Xi}^+ + \text{c.c.}$, $\psi(3686) \to K^-\Sigma^0\bar{\Xi}^+ + \text{c.c.}$, $\psi(3686) \to \gamma\chi_{cJ} \to \gamma K^-\Lambda\bar{\Xi}^+ + \text{c.c.}$ ($J = 0, 1, 2$), and $\psi(3686) \to \Xi(1690/1820)^-\bar{\Xi}^+ + \text{c.c.}$ with subsequent decay $\Xi(1690/1820)^- \to K^-\Lambda$ are measured for the first time.

DOI: 10.1103/PhysRevD.91.092006 PACS numbers: 13.25.Gv, 13.30.Eg, 14.20.Jn

I. INTRODUCTION

The quark model, an outstanding achievement of the last century, provides a rather good description of the hadron spectrum. However, baryon spectroscopy is far from complete, since many of the states expected in the SU(3) multiplets are either undiscovered or not well established [1], especially in the case of cascade hyperons with strangeness $S = -2$, the Ξ^*. Due to the small production cross sections and the complicated topology of the final states, only eleven Ξ^* states have been observed to date. Few of them are well established with spin parity determined, and most observations and measurements to date are from bubble chamber experiments or diffractive K^-p interactions [2].

As shown by the Particle Data Group (PDG), most Ξ^* hyperon results obtained to date have limited statistics [2]. For example, the $\Xi(1690)^-$ was first observed in the $\Sigma\bar{K}$ final state in the reaction $K^-p \to (\Sigma\bar{K})K\pi$ [3]. Afterwards its existence has been confirmed by other experiments [4–6], but its spin parity was not well determined. More recently, *BABAR* reported evidence for $J^P = 1/2^-$ for the $\Xi(1690)$ by analyzing the Legendre polynomial moments of the $\Xi^-\pi^+$ system in the decay $\Lambda_c^+ \to \Xi^-\pi^+K^+$ [7]. Clear evidence for $\Xi(1820)$ was observed in the $K^-\Lambda$ mass spectrum from a sample of 130 ± 16 events in K^-p interactions [8], and the $J = 1/2$ assumption was ruled out by using the Byers and Fenster technique [9]. Ten years later, a CERN-SPS experiment indicated that $\Xi(1820)$ favors negative parity in the case of $J = 3/2$ [10].

At present, the $\Xi(1690)$ and $\Xi(1820)$ are firmly established. Further investigation of their properties, e.g. mass, width and spin parity, is important to the understanding of Ξ^* states. Besides scattering experiments, decays from charmonium states offer a good opportunity to search for additional Ξ^* states. Although charmonium decays into pairs of $\Xi^{(*)}$ states are suppressed by the limited phase space, the narrow charmonium width which reduces the overlap with the neighboring states and the low background allows the investigation of these hyperons with high statistics charmonium samples.

Furthermore, our knowledge of charmonium decays into hadrons, especially to hyperons, is limited. The precise measurements of the branching fractions of charmonium decays may help provide a better understanding of the decay mechanism. The large $\psi(3686)$ data sample collected with the BESIII detector provides a good opportunity to study the cascade hyperons.

In this paper, we report on a study of the decays $\psi(3686) \to K^-\Lambda\bar{\Xi}^+ + \text{c.c.}$ and $\psi(3686) \to \gamma K^-\Lambda\bar{\Xi}^+ + \text{c.c.}$ based on a sample of $1.06 \times 10^8\, \psi(3686)$ events [11] collected with the BESIII detector. Another data sample, consisting of an integrated luminosity of 44.5 pb^{-1} [12] taken below the $\psi(3686)$ peak at $\sqrt{s} = 3.65$ GeV, is used to estimate continuum background. Evidence for the $\Xi(1690)^-$ and $\Xi(1820)^-$ is observed in the $K^-\Lambda$ invariant mass distribution in the decay $\psi(3686) \to K^-\Lambda\bar{\Xi}^+ + \text{c.c.}$ In the following, the charge conjugate decay mode is always implied unless otherwise specified.

II. DETECTOR AND MONTE CARLO SIMULATION

BEPCII is a two-ring collider designed for a luminosity of 10^{33} cm^{-2} s^{-1} at the $\psi(3770)$ resonance with a beam current of 0.93 A. The BESIII detector has a geometrical acceptance of 93% of 4π, and consists of a helium-gas-based drift chamber, a plastic scintillator time-of-flight system (TOF), a CsI(Tl) electromagnetic calorimeter (EMC), a superconducting solenoid magnet providing 1.0 T magnetic field, and a resistive plate chamber-based muon chamber. The momentum resolution of charged particles at 1 GeV/c is 0.5%. The time resolution of the TOF is 80 ps in the barrel detector and 110 ps in the end cap detectors. The photon energy resolution at 1 GeV is 2.5% (5%) in the barrel (end caps) of the EMC. The trigger system is designed to accommodate data taking at high

luminosity. A comprehensive description of the BEPCII collider and the BESIII detector is given in Ref. [13].

A GEANT4-based [14] Monte Carlo (MC) simulation software BOOST [15], which includes geometric and material description of the BESIII detector, detector response and digitization models as well as tracking of the detector running condition and performance, is used to generate MC samples. A series of exclusive MC samples, $\psi(3686)\to\gamma\chi_{cJ}\to\gamma K^-\Lambda\Xi^+$, $\psi(3686)\to K^-\Lambda\bar{\Xi}^+$, $\psi(3686)\to K^-\Sigma^0\bar{\Xi}^+$ are generated to optimize the selection criteria and estimate the corresponding selection efficiencies. The production of $\psi(3686)$ is simulated by the generator KKMC [16,17]. The decay $\psi(3686)\to\gamma\chi_{cJ}$ is assumed to be a pure $E1$ transition and to follow a $1+\alpha\cos^2\theta$ angular distribution with $\alpha=1$, $-1/3$ and $1/13$ for $J=0$, 1 and 2, respectively [18], where θ is the polar angle of the photon. The other subsequent decays are generated with BesEvtGen [19] with a uniform distribution in phase space. An inclusive MC sample, consisting of 1.06×10^8 $\psi(3686)$ events, is used to study potential backgrounds, where the known decay modes of $\psi(3686)$ are generated by BesEvtGen with branching fractions at world average values [2], and the remaining unknown decay modes are modeled by LUNDCHARM [20].

III. ANALYSIS OF $\psi(3686)\to K^-\Lambda\bar{\Xi}^+$

The decay $\psi(3686)\to K^-\Lambda\bar{\Xi}^+$ is reconstructed from the cascade decays $\Lambda\to p\pi^-$, $\bar{\Xi}^+\to\bar{\Lambda}\pi^+$ and $\bar{\Lambda}\to\bar{p}\pi^+$. At least six charged tracks are required and their polar angles θ must satisfy $|\cos\theta|<0.93$. The combined TOF and dE/dx information is used to form particle identification (PID) confidence levels for pion, kaon and proton hypotheses. Each track is assigned to the particle hypothesis type with the highest confidence level. Candidate events are required to have one kaon. If more than one kaon candidate is identified, only the kaon with the highest confidence level is kept, and the others are assumed to be pions. The same treatment is implemented for the proton and antiproton. The final identified charged kaon is further required to originate from the interaction point, i.e., the point of its closest approach to the beam is within 1 cm in the plane perpendicular to the beam and within ±10 cm along the beam direction.

In the analysis, constraints on the secondary decay vertices of the long-lived particles, Λ and $\bar{\Xi}^+$, are utilized to suppress backgrounds. Λ particles are reconstructed using secondary vertex fits [21] on $p\pi^-$ pairs. For events with more than one Λ candidate, the one with the smallest χ^2 for the secondary vertex fit is selected. $\bar{\Xi}^+$ candidates are reconstructed in two steps. A $\bar{p}\pi^+$ pair sharing a common vertex is selected to reconstruct the $\bar{\Lambda}$ candidate, and the common vertex is regarded as its decay vertex. The $\bar{\Xi}^+$ is then reconstructed with a $\bar{\Lambda}$ candidate and another π^+ by implementing another secondary vertex fit. For events with more than one $\bar{\Xi}^+$ candidate, the $\bar{p}\pi^+\pi^+$ combination with the minimum $|M(\bar{p}\pi^+)-M(\bar{\Lambda})|$ is selected, where $M(\bar{p}\pi^+)$ is the invariant mass of the $\bar{\Lambda}$ candidate from the secondary vertex fit, and $M(\bar{\Lambda})$ is the corresponding nominal mass from the PDG [2].

The selected K^-, Λ, and $\bar{\Xi}^+$ candidates are subjected to a four-momentum constraint kinematic fit (4C-fit) under the hypothesis of $\psi(3686)\to K^-\Lambda\bar{\Xi}^+$, and $\chi^2_{4C}<200$ is required to further suppress the potential backgrounds and to improve the resolution. Figure 1(a) shows the invariant mass distribution of $p\pi^-$, $M(p\pi^-)$, where a Λ peak is clearly visible. A mass window requirement $1.110<M(p\pi^-)<1.121$ GeV/c^2, corresponding to six times the mass resolution, is imposed to select Λ candidates. With the above selection criteria, the invariant mass of the $\bar{\Lambda}$ candidate $M(\bar{p}\pi^+)$ is shown in Fig. 1(b), and a clean $\bar{\Lambda}$ peak is observed. A mass window requirement $1.110<M(\bar{p}\pi^+)<1.121$ GeV/c^2 is applied to further improve the purity. Figure 1(c) shows the scatter plot of $M(p\pi^-)$ versus $M(\bar{\Lambda}\pi^+)$ without the Λ mass window requirement, where the accumulated events around the Λ-Ξ mass region are from the decay $\psi(3686)\to K^-\Lambda\bar{\Xi}^+$. The projection of $M(\bar{\Lambda}\pi^+)$ for all surviving events is shown in Fig. 1(d), where the $\bar{\Xi}^+$ peak is seen with very low background.

Potential non-$\bar{\Xi}^+$ backgrounds are studied with the $\psi(3686)$ inclusive MC sample by imposing the same selection criteria. The corresponding distribution of $M(\bar{\Lambda}\pi^+)$ is shown in Fig. 1(d) as the shaded histogram. The background is well described by the inclusive MC sample and is flat. Backgrounds are also investigated with the $M(p\pi^-)$ versus $M(\bar{p}\pi^+)$ two-dimensional sideband events from the data sample, where the sideband regions are defined as $1.102<M(p\pi^-/\bar{p}\pi^+)<1.107$ GeV/c^2 and $1.124<M(p\pi^-/\bar{p}\pi^+)<1.130$ GeV/c^2. No peaking structure is observed in the $M(\bar{\Lambda}\pi^+)$ distribution around the $\bar{\Xi}^+$ region. To estimate the nonresonant background coming directly from e^+e^- annihilation, the same selection criteria are implemented on the data sample taken at $\sqrt{s}=3.65$ GeV. Only one event with $M(\bar{\Lambda}\pi^+)$ at 1.98 GeV/c^2, located outside of the $\bar{\Xi}^+$ signal region, survives, which is normalized to an expectation of 3.6 events in $\psi(3686)$ data after considering the integrated luminosities and an assumed $1/s$ dependence of the cross section, as $L(\sqrt{s})\propto N_{\rm obs}/\sigma_{\rm QED}(\sqrt{s})$ [11], where L is the integrated luminosity and $\sigma_{\rm QED}$ is the cross section of QED processes. Therefore, the nonresonant background can be neglected.

A. BRANCHING FRACTION MEASUREMENT

To determine the event yield, an extended unbinned maximum likelihood fit is performed on the $M(\bar{\Lambda}\pi^+)$ distribution in Fig. 1(d). In the fit, the $\bar{\Xi}^+$ is described by a double Gaussian function, and the background is parametrized by a first order Chebychev polynomial function. The fit result, shown as the solid curve in

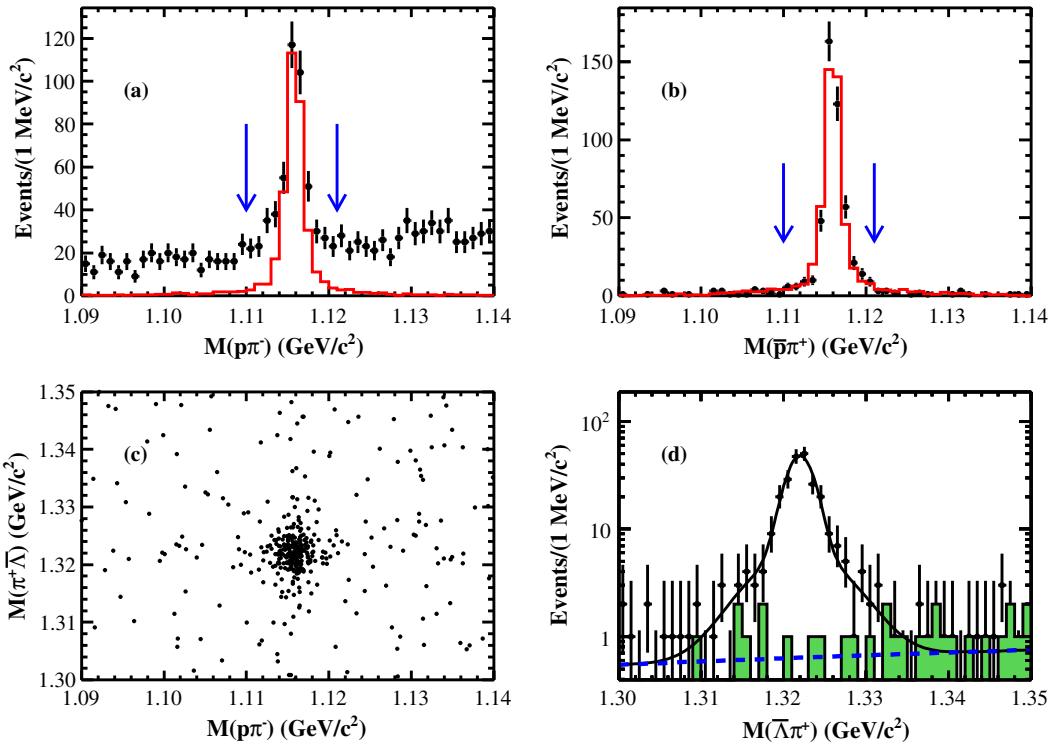

FIG. 1 (color online). Invariant mass distribution of (a) $p\pi^-$ and (b) $\bar{p}\pi^+$ (with the Λ mass window requirement). The arrows indicate the mass windows used in the analysis (see text). (c) Scatter plot of $M(p\pi^-)$ versus $M(\bar{\Lambda}\pi^+)$ for data. (d) $\bar{\Lambda}\pi^+$ invariant mass distribution. In the one-dimensional plots, the points with error bars are the data, the solid histograms are MC distributions normalized to the data, and the shaded histogram is the background estimated from the inclusive MC sample. The solid and long-dashed lines represent the fit curve and the background contribution from the fit.

Fig. 1(d), yields $N_{\rm obs} = 236.4 \pm 16.6\,\bar{\Xi}^+$ candidates. The decay branching fraction $\mathcal{B}(\psi(3686) \to K^-\Lambda\bar{\Xi}^+)$ is calculated to be

$$\mathcal{B}(\psi(3686) \to K^-\Lambda\bar{\Xi}^+) = \frac{N_{\rm obs}}{N_{\psi(3686)} \cdot \mathcal{B}^2(\Lambda \to p\pi^-) \cdot \mathcal{B}(\Xi^- \to \Lambda\pi^-) \cdot \epsilon} = (3.86 \pm 0.27) \times 10^{-5}, \quad (1)$$

where $N_{\psi(3686)} = (106.41 \pm 0.86) \times 10^6$ is the number of $\psi(3686)$ events determined with inclusive hadronic events [11], $\epsilon = 14.1\%$ is the detection efficiency, evaluated from the MC sample simulated with a uniform distribution in phase space, and $\mathcal{B}(\Lambda \to p\pi^-)$ and $\mathcal{B}(\bar{\Xi}^+ \to \bar{\Lambda}\pi^+)$ are the corresponding decay branching fractions [2]. The uncertainty is statistical only.

B. OBSERVATION OF Ξ^{*-} STATES

In the distribution of the $K^-\Lambda$ invariant mass, $M(K^-\Lambda)$, structures around 1690 and 1820 MeV/c^2, assumed to be $\Xi(1690)^-$ and $\Xi(1820)^-$, are evident with rather limited statistics. In order to improve the statistics, a partial reconstruction method is used where the K^- and Λ are required but the reconstruction of $\bar{\Xi}^+$ and the 4C kinematic fit are omitted. In addition, an identified antiproton is required among the remaining charged tracks to suppress background. With the above loose selection criteria, the distribution of $M(p\pi^-)$ is shown in Fig. 2(a), where a Λ is observed. After applying the $M(p\pi^-)$ mass window requirement, $1.110 < M(p\pi^-) < 1.121$ GeV/c^2, the distribution of the mass recoiling against the $K^-\Lambda$ system $RM(K^-\Lambda)$ is shown in Fig. 2(b), where the $\bar{\Xi}^+$ is observed, although with a higher background than in the full reconstruction. With a requirement of $1.290 < RM(K^-\Lambda) < 1.345\,\text{GeV}/c^2$, the $\Xi(1690)^-$ and $\Xi(1820)^-$ are observed in the $M(K^-\Lambda)$ distribution with improved statistics, as shown in Fig. 3. MC studies show that the event selection efficiency is improved by a factor of two using the partial reconstruction method.

To ensure that the observed structures are not from background, potential backgrounds are investigated using both data and inclusive MC samples. Non-$\Lambda(\bar{\Xi}^+)$ background is estimated from the events in the $\Lambda(\bar{\Xi}^+)$ sideband regions, defined as $1.102 < M(p\pi^-) < 1.107$ GeV/c^2 and $1.124 < M(p\pi^-) < 1.130$ GeV/c^2 ($1.243 < RM(K^-\Lambda) < 1.270$ GeV/c^2 and $1.365 < RM(K^-\Lambda) < 1.393$ GeV/c^2), and their $M(K^-\Lambda)$ distribution is shown in Fig. 3 with the dot-dashed (dashed) histogram. Possible background sources are also investigated with the inclusive MC sample,

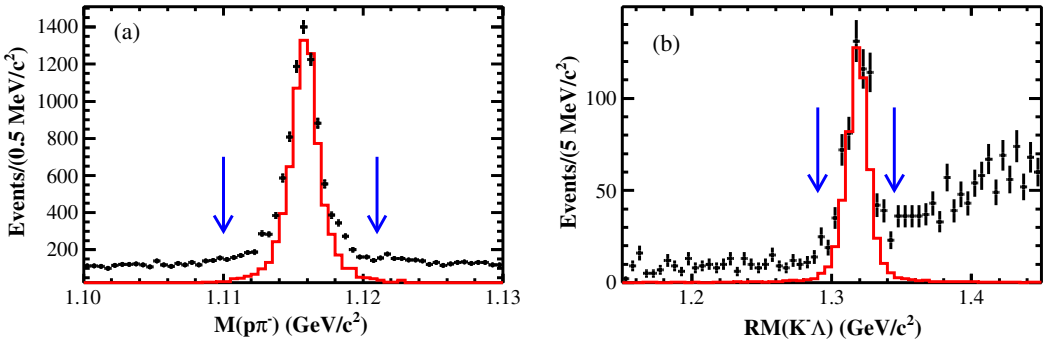

FIG. 2 (color online). Invariant mass spectrum (a) of $p\pi^-$, and (b) of the mass recoiling against the $K^-\Lambda$ system. The dots with error bars show the distribution for data, and the solid histogram shows that for the exclusive MC normalized to the data in the signal region. The arrows indicate the selection region used in the analysis (see text).

and the result is shown with the shaded histogram in Fig. 3. No evidence of peaking structures in the $M(K^-\Lambda)$ distribution is observed in either the sideband region or the inclusive MC sample. The same selection criteria are applied to the data sample collected at 3.65 GeV to estimate the background coming directly from e^+e^- annihilation. Only one event with $M(K^-\Lambda)$ around 1.98 GeV survives, which corresponds to an expected 3.6 events when normalized to the $\psi(3686)$ sample. This background can therefore be neglected.

An extended unbinned maximum likelihood fit of the $M(K^-\Lambda)$ distribution is performed to determine the resonance parameters and event yields of the excited Ξ^{*-} hyperons. In the fit, the Ξ^{*-} shapes are described by Breit-Wigner functions $A_i(m)$ convoluted with Gaussian functions $G(m,\mu,\sigma)$, which represent the mass shift and resolution in the reconstruction, multiplied by the mass dependent efficiency $\varepsilon(m)$, $\varepsilon(m)[G(m,\mu_i,\sigma_i)\otimes A_i^2(m)]$. In the fit, both parameters of $G(m,\mu,\sigma)$ and $\varepsilon(m)$ are fixed as the values determined from the studies to exclusive MC samples, and the Breit-Wigner function $A_i(m)$ is described below. The shape of the background is parametrized by a function $B(m)=(m-m_0)^{1/2}+c(m-m_0)^{3/2}$, where m_0 is the mass threshold and c is a free parameter.

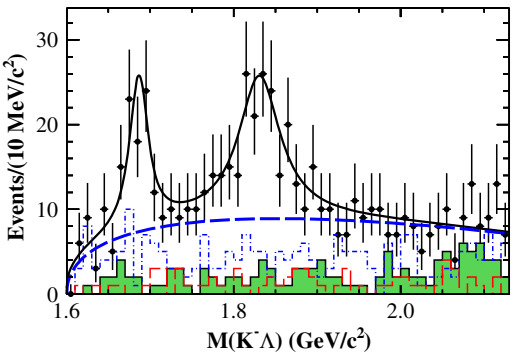

FIG. 3 (color online). Invariant $K^-\Lambda$ mass distribution. Points with error bars represent data, and the solid and dashed curves are the fit curve and the nonresonant contribution obtained from the fit. The shaded histogram represents the background estimated from the inclusive MC sample, and the dashed and dot-dashed histograms are the Λ sideband and the $\bar{\Xi}^+$ sideband backgrounds from data, respectively.

The Breit-Wigner function $A_i(m)$ used in the fit can be written as

$$A(m)=\frac{p_\Lambda(m)^{(L_{(K^-\Lambda)}+1/2)}p_{\bar{\Xi}^+}(m)^{(L_{(\Xi^{*-}\bar{\Xi}^+)}+1/2)}}{m-M+i\frac{\Gamma}{2}}\cdot\left(\frac{B_{L_{(K^-\Lambda)}}(p_\Lambda(m))}{B_{L_{(K^-\Lambda)}}(p'_\Lambda)}\right)\left(\frac{B_{L_{(\Xi^{*-}\bar{\Xi}^+)}}(p_{\bar{\Xi}^+}(m))}{B_{L_{(\Xi^{*-}\bar{\Xi}^+)}}(p'_{\bar{\Xi}^+})}\right),\qquad(2)$$

where M, Γ are the mass and width of the Ξ^{*-}, the $p_\Lambda(m)(p_{\bar{\Xi}^+}(m))$ is the available momentum of $\Lambda(\bar{\Xi}^+)$ in the center-of-mass frame of $\Xi^*(\psi(3686))$ at mass m, $p'_\Lambda(p'_{\bar{\Xi}^+})$ is $p_\Lambda(m)(p_{\bar{\Xi}^+}(m))$ for $m=M$, and L is the orbital angular momentum. Due to the limited statistics, we do not determine the spin parities of $\Xi(1690)^-$ and $\Xi(1820)^-$ with this data sample. In the fit, the spin parities of $\Xi(1690)^-$ and $\Xi(1820)^-$ are assumed to be $J^P=1/2^-$ and $J^P=3/2^-$ based on previous experimental results [7,8], the $\Xi^{*-}\bar{\Xi}^+$ angular momenta ($L_{(\Xi^{*-}\bar{\Xi}^+)}$) are set to be 0 for both the $\Xi(1690)^-$ and $\Xi(1820)^-$, while the $K^-\Lambda$ angular momenta ($L_{(K^-\Lambda)}$) are 0 and 2 respectively. $B_L(p)$ is the Blatt-Weisskopf form factor [22]:

$$B_0(p)=1;\qquad B_2(p)=\sqrt{\frac{13}{p^4+3p^2Q_0^2+9Q_0^4}},\qquad(3)$$

where Q_0 is a hadron "scale" parameter which is on the order of 1 fm [22], and was set to be 0.253 GeV/c in the fit according to the result of the FOCUS experiment [23].

The overall fit result and the background components from the fit are shown as the solid and dashed curves in Fig. 3, respectively. The resulting masses, widths and event yields, as well as the corresponding significances of the $\Xi(1690)^-$ and $\Xi(1820)^-$ signals, are summarized in Table I, where the significance is evaluated by comparing the difference of log-likelihood values with and without the $\Xi^-(1690/1820)$ included in the fit and taking the change

TABLE I. $\Xi(1690)^-$ and $\Xi(1820)^-$ fit results, where the first uncertainty is statistical and the second systematic. The $\mathcal{B}$ denotes the product branching fraction $\mathcal{B}(\psi(3686) \to \Xi(1690/1820)^-\bar{\Xi}^+) \times \mathcal{B}(\Xi(1690/1820)^- \to K^-\Lambda)$.

	$\Xi(1690)^-$	$\Xi(1820)^-$
$M(\mathrm{MeV}/c^2)$	$1687.7 \pm 3.8 \pm 1.0$	$1826.7 \pm 5.5 \pm 1.6$
$\Gamma(\mathrm{MeV})$	$27.1 \pm 10.0 \pm 2.7$	$54.4 \pm 15.7 \pm 4.2$
Event yields	74.4 ± 21.2	136.2 ± 33.4
Significance(σ)	4.9	6.2
Efficiency(%)	32.8	26.1
$\mathcal{B}(10^{-6})$	$5.21 \pm 1.48 \pm 0.57$	$12.03 \pm 2.94 \pm 1.22$
$M_{\mathrm{PDG}}(\mathrm{MeV}/c^2)$	1690 ± 10	1823 ± 5
$\Gamma_{\mathrm{PDG}}(\mathrm{MeV})$	< 30	24^{+15}_{-10}

of the number of degrees of freedom into consideration. The significance is calculated when studying the systematic uncertainty sources (Sec. V) and the smallest value is reported here. The resonance parameters from the PDG [2] are also listed in Table I for comparison.

Due to the limited statistics, the measurement of spin parity of $\Xi(1690/1820)^-$ is not performed in this analysis. To determine the product branching fractions of the cascade decay $\mathcal{B}(\psi(3686) \to \Xi(1690/1820)^-\bar{\Xi}^+) \times \mathcal{B}(\Xi(1690/1820)^- \to K^-\Lambda)$, the corresponding detection efficiencies are evaluated with MC samples taking the spin parity of $\Xi(1690)^-$ and $\Xi(1820)$ to be $J^P = 1/2^-$ and $3/2^-$, respectively. The detection efficiencies and the corresponding product branching fractions are also listed in Table I. Corresponding systematic uncertainties are evaluated in Sec. V.

IV. ANALYSIS OF $\psi(3686) \to \gamma K^-\Lambda\bar{\Xi}^+$

In this analysis, the same selection criteria as those used in the $\psi(3686) \to K^-\Lambda\bar{\Xi}^+$ analysis are implemented to select the K^- and to reconstruct Λ and $\bar{\Xi}^+$ candidates. Photon candidates are reconstructed from isolated showers in EMC crystals, and the energy deposited in the nearby TOF counters is included to improve the photon reconstruction efficiency and the energy resolution. A good photon is required to have a minimum energy of 25 MeV in the EMC barrel region ($|\cos(\theta)| < 0.8$) and 50 MeV in the end cap region ($0.86 < |\cos(\theta)| < 0.92$). A timing requirement ($0 \le t \le 700$ ns) is applied to further suppress electronic noise and energy deposition unrelated to the event. The photon candidate is also required to be isolated from all charged tracks by more than 10°.

The selected photons, K^-, and Λ and $\bar{\Xi}^+$ candidates are subjected to a 4C-fit under the hypothesis of $\psi(3686) \to \gamma K^-\Lambda\bar{\Xi}^+$, and $\chi^2_{4C} < 100$ is required. For events with more than one good photon, the one with the minimum χ^2_{4C} is selected. MC studies show that the background arising from $\psi(3686) \to K^-\Lambda\bar{\Xi}^+$ can be effectively rejected by the 4C-fit and the χ^2_{4C} requirement.

With the above selection criteria, the $M(p\pi^-)$ distribution is shown in Fig. 4(a). The Λ is observed clearly with

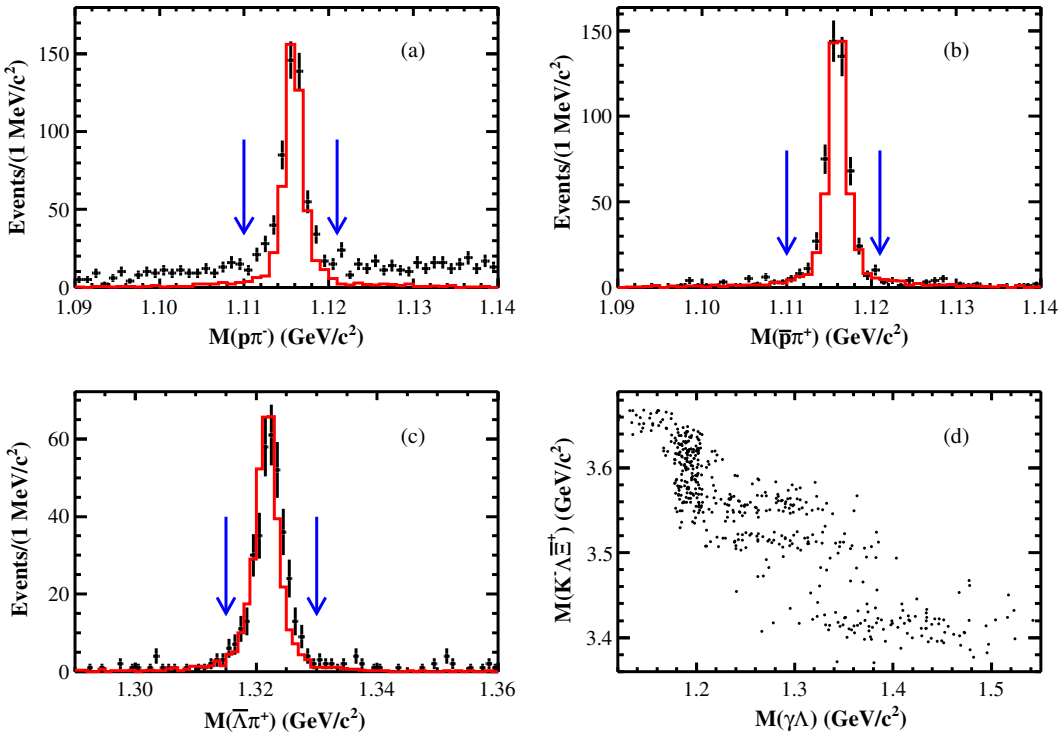

FIG. 4 (color online). The invariant mass distributions of (a) $p\pi^-$, (b) $\bar{p}\pi^+$ (with the Λ selected) and (c) $\bar{\Lambda}\pi^+$. Dots with error bars are data, and the solid histogram is from the phase-space MC, which is normalized to the data. The arrows indicate the selection requirements used in the analysis (see text). (d) The scatter plot of $M(\gamma\Lambda)$ versus $M(K^-\Lambda\bar{\Xi}^+)$ for data.

low background, and the requirement $1.110 < M(p\pi^-) < 1.121$ GeV/c^2 is used to select Λ candidates. After that, the distribution of $M(\bar{p}\pi^+)$ is shown in Fig. 4(b), where the $\bar{\Lambda}$ is observed with almost no background. The requirement $1.110 < M(\bar{p}\pi^+) < 1.121$ GeV/c^2 is further applied to improve the purity. The $M(\bar{\Lambda}\pi^+)$ distribution of the surviving events is shown in Fig. 4(c), and a mass window requirement $1.315 < M(\bar{\Lambda}\pi^+) < 1.330$ GeV/c^2 is used to select $\psi(3686) \to \gamma K^-\Lambda\bar{\Xi}^+$ candidates. Figure 4(d) shows the scatter plot of $M(\gamma\Lambda)$ versus $M(K^-\Lambda\bar{\Xi}^+)$ with all the above selection criteria. The vertical band around the Σ^0 mass is from the decay $\psi(3686) \to K^-\Sigma^0\bar{\Xi}^+$, while three horizontal bands around the χ_{cJ} $(J = 0, 1, 2)$ mass regions are from $\psi(3686) \to \gamma\chi_{cJ}, \chi_{cJ} \to K^-\Lambda\bar{\Xi}^+ (J = 0, 1, 2)$. There is also a horizontal band around the $\psi(3686)$ mass region, which is background from $\psi(3686) \to K^-\Lambda\bar{\Xi}^+$ with a random photon candidate.

A. STUDY OF $\psi(3686) \to K^-\Sigma^0\bar{\Xi}^+$

After applying all the above selection criteria, the projection of $M(\gamma\Lambda)$ is shown in Fig. 5, where a clear Σ^0 peak is visible with low backgrounds. As shown in Fig. 4(d), the cascade process of $\psi(3686) \to \gamma\chi_{c2}$, $\chi_{c2} \to K^-\Lambda\bar{\Xi}^+$ will overlap with the Σ^0 band on $M(\gamma\Lambda)$. This process is investigated as potential background using the inclusive MC sample together with the exclusive process $\psi(3686) \to \pi^+\pi^- J/\psi$, $J/\psi \to K^- p\bar{\Sigma}^0$. Both processes have the same final states as the signal, but do not produce a peak in the $M(\gamma\Lambda)$ distribution around the Σ^0 region. The distribution of background obtained from the inclusive MC sample is shown as the shaded histogram in Fig. 5. The background is also studied with the candidate events within the Λ or $\bar{\Xi}^+$ sideband regions of data, and the lack of peaking background in the $M(\gamma\Lambda)$ distribution is confirmed. The background from e^+e^- annihilation directly is estimated by imposing the same selection criteria on the data sample taken at $\sqrt{s} = 3.65$ GeV. No event survives, and this background is negligible.

To determine the $\psi(3686) \to K^-\Sigma^0\bar{\Xi}^+$ yield, an extended unbinned maximum likelihood fit of the $M(\gamma\Lambda)$ distribution is performed with a double Gaussian function for the Σ^0 together with a first order Chebychev polynomial for the background shape. The overall fit result and the background component are shown in Fig. 5 with solid and dashed lines, respectively. The fit yields the number of Σ^0 events to be 142.5 ± 13.0, and the resulting branching fraction to be $\mathcal{B}(\psi(3686) \to K^-\Sigma^0\bar{\Xi}^+) = (3.67 \pm 0.33) \times 10^{-5}$, by taking the detection efficiency of 9.0% obtained from MC simulation and the branching fractions of intermediate states [2] into consideration. The errors are statistical only.

B. STUDY OF $\chi_{cJ} \to K^-\Lambda\bar{\Xi}^+ (J = 0,1,2)$

The $\chi_{cJ} \to K^-\Lambda\bar{\Xi}^+ (J = 0, 1, 2)$ yields are determined by fitting the invariant mass distribution of $K^-\Lambda\bar{\Xi}^+$, $M(K^-\Lambda\bar{\Xi}^+)$. To remove the background from $\psi(3686) \to K^-\Sigma^0\bar{\Xi}^+$, the additional selection $M(\gamma\Lambda) > 1.21$ GeV/c^2 is applied. The $M(K^-\Lambda\bar{\Xi}^+)$ distribution is shown in Fig. 6, where the χ_{cJ} peaks are observed clearly. Potential backgrounds are studied using the events in the Λ or $\bar{\Xi}^+$ sideband regions of data and the inclusive MC samples. The inclusive MC $M(K^-\Lambda\bar{\Xi}^+)$ distribution is shown in Fig. 6 as the shaded histogram. According to the MC study, the dominant backgrounds are from the cascade decays $\psi(3686) \to \pi^+\pi^- J/\psi, J/\psi \to pK^-\bar{\Sigma}^0$, $\bar{\Sigma}^0 \to \gamma\bar{\Lambda}$ and $\psi(3686) \to K^- p\pi^-\bar{p}\pi^+\pi^+$, but none of them produces peak in the χ_{cJ} regions.

An extended unbinned maximum likelihood fit of the $M(K^-\Lambda\bar{\Xi}^+)$ distribution is performed to determine the number of χ_{cJ} events. The χ_{cJ} resonances are described by Breit-Wigner functions convoluted with Gaussian functions to account for the mass resolution, and the background is described by a first order Chebychev polynomial function.

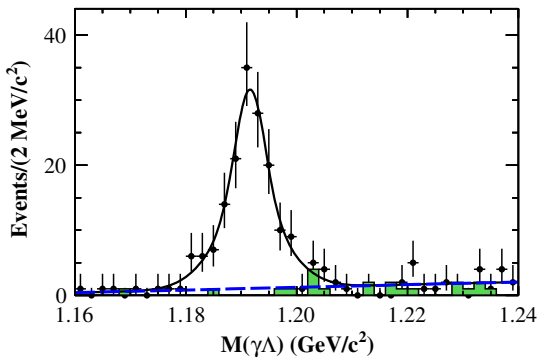

FIG. 5 (color online). The $M(\gamma\Lambda)$ distribution, where the dots with error bars are data, the shaded histogram is the background contribution estimated from the inclusive MC sample, and the solid and dashed lines are the fit results for the overall and background components, respectively.

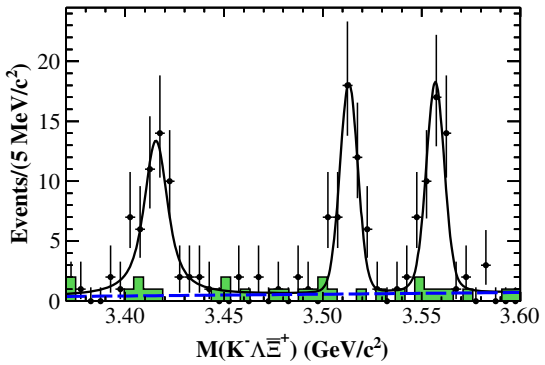

FIG. 6 (color online). The $K^-\Lambda\bar{\Xi}^+$ mass distribution, where the dots with error bars are data, the shaded histogram is the background contribution estimated from the inclusive MC sample, and the solid and dashed lines are the overall and background component contributions from the fit.

The fit results are shown as the solid curve in Fig. 6, and the yields of $\chi_{cJ}(J=0,1,2)$ are 56.9 ± 8.9, 48.5 ± 7.4 and 50.8 ± 7.8 events, respectively. Taking the detection efficiencies, 6.9%, 8.5% and 6.9% for $\chi_{cJ}(J=0,1,2)$ estimated by MC simulation, and the branching fractions of the decays of intermediate states [2] into consideration, the product branching fractions $\mathcal{B}(\psi(3686)\to\gamma\chi_{cJ})\times\mathcal{B}(\chi_{cJ}\to K^-\Lambda\bar{\Xi}^+)$ are measured to be $(1.90\pm0.30)\times10^{-5}$, $(1.32\pm0.20)\times10^{-5}$ and $(1.68\pm0.26)\times10^{-5}$ for χ_{cJ} $(J=0,1,2)$, respectively. The errors are statistical only.

V. SYSTEMATIC UNCERTAINTY

The different sources of systematic uncertainties for the measurement of branching fractions are considered and described below.

(a) Tracking efficiency

In the analysis, both the proton and pion are from long-lived particles (Λ or Ξ^-), and the corresponding tracking efficiencies are studied using a clean Λ control sample, selected by requiring the invariant mass recoiling against the $\bar{p}K^+$ system to be within the Λ mass region in the decay $J/\psi\to\Lambda\bar{p}K^+$. The invariant mass recoiling against the $\bar{p}K^+\pi^-(\bar{p}K^+p)$ system is further required to be within the proton (pion) mass region to improve the purity of the control sample. The uncertainty of the tracking efficiency is estimated by the difference between efficiencies in data and MC samples and is parametrized as a function of transverse momentum. The average uncertainty of the proton (pion) tracking efficiency is estimated to be 1% (1%) by weighting with the transverse momentum distribution of the signal. The uncertainty of the $K^\pm$ tracking efficiency is studied with a clean control sample of $J/\psi\to K^*(892)^0K^0_S$, $K^*(892)^0\to K^\pm\pi^\mp$, and the systematic uncertainty is estimated to be 1% [24].

(b) PID efficiency

Similarly, the PID efficiencies of $p/\bar{p}$ and $K^\pm$ are estimated using the same control samples as those in tracking efficiency studies. All tracks are reconstructed and the target one is allowed to be unidentified. The systematic uncertainties for p, $\bar{p}$ and $K^\pm$ are all found to be 1%.

(c) Photon detection efficiency

The photon detection efficiency is studied utilizing the control samples $\psi(3686)\to\pi^+\pi^-J/\psi$, $J/\psi\to\rho^0\pi^0$ and $\psi(3686)\to\pi^0\pi^0J/\psi$ with $J/\psi\to l^+l^-(l=e,\mu)$ and $\rho^0\pi^0$. The corresponding systematic uncertainty is estimated by the difference of detection efficiency between data and MC samples, and 1% is assigned for each photon [25].

(d) The secondary vertex fit

The efficiencies of the secondary vertex fits for Λ and Ξ^- are investigated by the control samples $J/\psi\to\Lambda\bar{p}K^+$ and $J/\psi\to\Xi^-\bar{\Xi}^+$. The differences of efficiencies between data and MC samples are found to be 1%, and are taken as the systematic uncertainties.

(e) Kinematic fit

The track helix parameters (ϕ_0, κ, $\tan\lambda$) for MC samples are corrected to reduce the difference of the χ^2_{4C} distributions between data and MC [26]. The corresponding correction factors for kaons and the tracks from Λ decay (proton and pion) are obtained from a clean sample $J/\psi\to\Lambda\bar{p}K^+$, and those for the tracks from Ξ^- decay are obtained from the sample $J/\psi\to\Xi^-\bar{\Xi}^+$. The systematic uncertainties related to the 4C-fit, 1%, are estimated by the difference of efficiency between MC samples with and without the track helix parameter corrections.

(f) The fit method

The systematic uncertainties related to the fit method are considered according to the following aspects. (1) The signal line shapes: In the measurements of $\mathcal{B}(\psi(3686)\to K^-\Lambda\bar{\Xi}^+)$, $\mathcal{B}(\chi_{cJ}\to K^-\Lambda\bar{\Xi}^+)$ and $\mathcal{B}(\psi(3686)\to K^-\Sigma^0\bar{\Xi}^+)$, the signal line shapes are replaced by alternative fits using MC shapes, and the changes of yields are assigned as the systematic uncertainties. In the measurements of $\mathcal{B}(\psi(3686)\to\Xi^{*-}\bar{\Xi}^+)$, the corresponding uncertainties mainly come from the uncertainty of Q_0. Alternative fits varying the Q_0 values within one standard deviation [23] are performed, and the changes of yields are treated as the systematic uncertainties. (2) The background line shapes: In the measurements of $\mathcal{B}(\psi(3686)\to K^-\Lambda\bar{\Xi}^+)$, $\mathcal{B}(\chi_{cJ}\to K^-\Lambda\bar{\Xi}^+)$ and $\mathcal{B}(\psi(3686)\to K^-\Sigma^0\bar{\Xi}^+)$, the background shapes are described with a first order Chebychev polynomial function in the fit. Alternative fits with a second order Chebychev polynomial function are performed, and the resulting differences of the yields are taken as the systematic uncertainties related to the background line shapes. In the measurement of $\mathcal{B}(\psi(3686)\to\Xi^{*-}\bar{\Xi}^+)$, an alternative fit with a reversed ARGUS function (rARGUS),[1] $F_{\rm rARGUS}(m)=F_{\rm ARGUS}(2m_0-m)$, for the nonresonant components is performed, where m_0 is the mass threshold of $K^-\Lambda$. The changes in the yields are taken as systematic uncertainties. (3) Fit range: Fits with varied fit ranges, i.e., varied by expanding/contracting the range by 10 MeV/c^2 and shifting left and right by 10 MeV/c^2, are performed. The resulting largest differences are treated as the systematic uncertainties. (4) Mass shift and resolution difference: In the measurement of branching fractions related to Ξ^{*-}, a Gaussian function $G(m,\mu,\sigma)$, which represents the Ξ^{*-} mass resolution, is included in the

[1]The ARGUS function is defined as $F_{\rm ARGUS}(m;m_0,c,p)=m(1-(\frac{m}{m_0})^2)^p\cdot\exp(c(1-(\frac{m}{m_0})^2))$, where m_0 is the mass threshold and c and p are parameters fixing the shape

TABLE II. Summary of the relative systematic uncertainties (in %) in the branching fraction measurements. Here $K\Lambda\Xi$, $K\Sigma^0\Xi$, χ_{cJ} and $\Xi^{*-}\bar{\Xi}^+$ denote $\psi(3686)\to K^-\Lambda\bar{\Xi}^+$, $\psi(3686)\to K^-\Sigma^0\bar{\Xi}^+$, $\psi(3686)\to\gamma\chi_{cJ},\chi_{cJ}\to K^-\Lambda\bar{\Xi}^+$ and $\psi(3686)\to\Xi(1690/1820)^-\bar{\Xi}^+$, $\Xi(1690/1820)^-\to K^-\Lambda$, respectively.

Source	$K\Lambda\Xi$	$K\Sigma^0\Xi$	χ_{cJ}	$\Xi^{*-}\bar{\Xi}^+$
Tracking	6	6	6	4
PID	3	3	3	3
Λ vertex fit	1	1	1	1
Ξ vertex fit	1	1	1	...
Kinematic fit	1	1	1	...
Photon detection	...	1	1	...
Signal model	2.1	0.5	1.1,3.0,2.4	0.8,1.6
Background shape	1.6	0.5	0,1.5,0.6	7.1,7.1
Fit range	1.6	1.9	0.2,0.1,0.2	6.3,4.4
Mass shift, resolution	...	...	...	0.6,0.4
Mass windows	2.9	1.4	3.2,2.3,1.8	1.0,1.3
$\mathcal{B}(\Lambda\to p\pi^-)$	0.8	0.8	0.8	0.8
$\mathcal{B}(\bar{\Xi}^+\to\bar{\Lambda}\pi^+)$	0.035	0.035	0.035	0.035
$\mathcal{B}(\bar{\Lambda}\to\bar{p}\pi^+)$	0.8	0.8	0.8	0.8
$\mathcal{B}(\psi(3686)\to\gamma\chi_{cJ})$	...	...	3.2,4.3,4.0	...
$N_{\psi(3686)}$	0.8	0.8	0.8	0.8
Total	8.2	7.6	8.5,9.3,8.7	11.0,10.1

fit, where the parameters of the Gaussian function are evaluated from MC simulation. To estimate the systematic uncertainty related to the mass shift and resolution difference between data and MC simulation, a fit with a new Gaussian function with additional parameters, i.e., $G(m,\mu+\Delta\mu,\sigma+\Delta\sigma)$, is performed, and the resulting difference is taken as the systematic uncertainty. The additional values $\Delta\mu$ and $\Delta\sigma$ are estimated by the difference in the fit results of the Λ and $\bar{\Xi}^+$ between data and MC simulation.

(g) Mass window requirement

The systematic uncertainties related to Λ and $\bar{\Xi}^+$ mass window requirements are estimated by varying the size of the mass window, i.e. contracting/expanding by 2 MeV/c^2. The resulting differences of branching fractions are treated as the systematic uncertainties.

(h) Other

The systematic uncertainties of the branching fractions of the decays $\psi(3686)\to\gamma\chi_{cJ}$, $\Xi^-\to\Lambda\pi^-$ and $\Lambda\to p\pi^-$ are taken from the world average values [2]. The uncertainty in the number of $\psi(3686)$ events is 0.8%, which is obtained by studying inclusive $\psi(3686)$ decays [11]. The uncertainty in the trigger efficiency is found to be negligible due to the large number of charged tracks [27].

The different sources of systematic uncertainties in the measured branching fractions are summarized in Table II. Assuming all of the uncertainties are independent, the total systematic uncertainties are obtained by adding the individual uncertainties in quadrature.

In the measurement of the Ξ^{*-} resonance parameters, the sources of systematic uncertainty related to the fit method and the Λ and $\bar{\Xi}^+$ mass window requirements are considered. The same methods as those used above are implemented, and the differences of the mass and width of Ξ^{*-} are regarded as the systematic uncertainties and are summarized in Table III. The total systematic uncertainties on Ξ^{*-} resonance parameters obtained by adding the individual uncertainties in quadrature are shown in Table III.

TABLE III. Summary of the systematic uncertainties on Ξ^{*-} parameters.

	$\Xi(1690)^-$		$\Xi(1820)^-$	
	M(MeV/c^2)	Γ(MeV)	M(MeV/c^2)	Γ(MeV)
Signal model	0.2	0.3	1.5	1.2
Background shape	0.3	1.8	0.5	3.3
Fit range	0.3	1.7	0.2	2.2
Mass shift, resolution	0.5	0.8	0.2	0.2
Mass windows	0.7	0.7	0.4	0.6
Total	1.0	2.7	1.6	4.2

VI. CONCLUSION

Using a sample of 1.06×10^8 $\psi(3686)$ events collected with the BESIII detector, the processes of $\psi(3686)\to K^-\Lambda\bar{\Xi}^+$ and $\psi(3686)\to\gamma K^-\Lambda\bar{\Xi}^+$ are studied for the first time. In the decay $\psi(3686)\to K^-\Lambda\bar{\Xi}^+$, the branching fraction $\mathcal{B}(\psi(3686)\to K^-\Lambda\bar{\Xi}^+)$ is measured, and two structures, around 1690 and 1820 MeV/c^2, are observed in the $K^-\Lambda$ invariant mass spectrum with significances of 4.9σ and 6.2σ, respectively. The fitted resonance parameters are consistent with those of $\Xi^-(1690)$ and $\Xi^-(1820)$ in the PDG [2] within one standard deviation. The measured masses, widths, and product decay branching fractions $\mathcal{B}(\psi(3686)\to\Xi^{*-}\bar{\Xi}^+)\times\mathcal{B}(\Xi^{*-}\to K^-\Lambda)$ are summarized in Table I. This is the first time that $\Xi^-(1690)$ and $\Xi^-(1820)$ hyperons have been observed

TABLE IV. Summary of the branching fractions measurements, where the first uncertainty is statistical and the second systematic.

Decay	Branching fraction
$\psi(3686)\to K^-\Lambda\bar{\Xi}^+$	$(3.86\pm0.27\pm0.32)\times10^{-5}$
$\psi(3686)\to\Xi(1690)^-\bar{\Xi}^+$, $\Xi(1690)^-\to K^-\Lambda$	$(5.21\pm1.48\pm0.57)\times10^{-6}$
$\psi(3686)\to\Xi(1820)^-\bar{\Xi}^+$, $\Xi(1820)^-\to K^-\Lambda$	$(12.03\pm2.94\pm1.22)\times10^{-6}$
$\psi(3686)\to K^-\Sigma^0\bar{\Xi}^+$	$(3.67\pm0.33\pm0.28)\times10^{-5}$
$\psi(3686)\to\gamma\chi_{c0},\chi_{c0}\to K^-\Lambda\bar{\Xi}^+$	$(1.90\pm0.30\pm0.16)\times10^{-5}$
$\psi(3686)\to\gamma\chi_{c1},\chi_{c1}\to K^-\Lambda\bar{\Xi}^+$	$(1.32\pm0.20\pm0.12)\times10^{-5}$
$\psi(3686)\to\gamma\chi_{c2},\chi_{c2}\to K^-\Lambda\bar{\Xi}^+$	$(1.68\pm0.26\pm0.15)\times10^{-5}$
$\chi_{c0}\to K^-\Lambda\bar{\Xi}^+$	$(1.96\pm0.31\pm0.16)\times10^{-4}$
$\chi_{c1}\to K^-\Lambda\bar{\Xi}^+$	$(1.43\pm0.22\pm0.12)\times10^{-4}$
$\chi_{c2}\to K^-\Lambda\bar{\Xi}^+$	$(1.93\pm0.30\pm0.15)\times10^{-4}$

in charmonium decays. In the study of the decay $\psi(3686) \to \gamma K^- \Lambda \bar{\Xi}^+$, the branching fractions $\mathcal{B}(\psi(3686) \to K^- \Sigma^0 \bar{\Xi}^+)$ and $\mathcal{B}(\chi_{cJ} \to K^- \Lambda \bar{\Xi}^+)$ are measured. All of the measured branching fractions are summarized in Table IV. The measurements provide new information on charmonium decays to hyperons and on the resonance parameters of the hyperons, and may help in the understanding of the charmonium decay mechanism.

ACKNOWLEDGMENTS

The BESIII collaboration thanks the staff of BEPCII and the IHEP computing center for their strong support. This work is supported in part by National Key Basic Research Program of China under Contract No. 2015CB856700; Joint Funds of the National Natural Science Foundation of China under Contracts No. 11079008, No. 11179007, No. U1232201, and No. U1332201; National Natural Science Foundation of China (NSFC) under Contracts No. 10935007, No. 11121092, No. 11125525, No. 11235011, No. 11322544, No. 11335008, No. 11375204, and No. 11275210; the Chinese Academy of Sciences (CAS) Large-Scale Scientific Facility Program; CAS under Contracts No. KJCX2-YW-N29 and No. KJCX2-YW-N45; 100 Talents Program of CAS; INPAC and Shanghai Key Laboratory for Particle Physics and Cosmology; German Research Foundation DFG under Collaborative Research Center Contract No. CRC-1044; Istituto Nazionale di Fisica Nucleare, Italy; Ministry of Development of Turkey under Contract No. DPT2006K-120470; Russian Foundation for Basic Research under Contract No. 14-07-91152; U.S. Department of Energy under Contracts No. DE-FG02-04ER41291, No. DE-FG02-05ER41374, No. DE-FG02-94ER40823, and No. DESC0010118; U.S. National Science Foundation; University of Groningen (RuG) and the Helmholtzzentrum fuer Schwerionenforschung GmbH (GSI), Darmstadt; WCU Program of National Research Foundation of Korea under Contract No. R32-2008-000-10155-0.

[1] R. Horgan, Nucl. Phys. **B71**, 514 (1974); M. Jones, R. H. Dalitz, and R. Horgan, Nucl. Phys. **B129**, 45 (1977).
[2] K. A. Olive *et al.*, Chin. Phys. C **38**, 090001 (2014).
[3] C. Dionisi *et al.*, Phys. Lett. B **80**, 145 (1978).
[4] S. F. Biagi *et al.*, Z. Phys. C **9**, 305 (1981); S. F. Biagi *et al.*, Z. Phys. C **34**, 15 (1987).
[5] M. I. Adamovich *et al.* (WA89 Collaboration), Eur. Phys. J. C **5**, 621 (1998).
[6] K. Abe *et al.* (Belle Collaboration), Phys. Lett. B **524**, 33 (2002).
[7] B. Aubert *et al.* (*BABAR* Collaboration), Phys. Rev. D **78**, 034008 (2008).
[8] J. B. Gay *et al.*, Phys. Lett. B **62**, 477 (1976).
[9] N. Byers and S. Fenster, Phys. Rev. Lett. **11**, 52 (1963).
[10] S. F. Biagi *et al.*, Z. Phys. C **34**, 175 (1987).
[11] M. Ablikim *et al.* (BESIII Collaboration), Chin. Phys. C **37**, 063001 (2013).
[12] M. Ablikim *et al.* (BESIII Collaboration), Chin. Phys. C **37**, 123001 (2013).
[13] M. Ablikim *et al.* (BESIII Collaboration), Nucl. Instrum. Methods Phys. Res., Sect. A **614**, 345 (2010).
[14] S. Agostinelli *et al.* (GEANT4 Collaboration), Nucl. Instrum. Methods Phys. Res., Sect. A **506**, 250 (2003).
[15] Z. Y. Deng *et al.*, Chin. Phys. C **30**, 371 (2006).
[16] S. Jadach, B. F. L. Ward, and Z. Was, Comput. Phys. Commun. **130**, 260 (2000).
[17] S. Jadach, B. F. L. Ward, and Z. Was, Phys. Rev. D **63**, 113009 (2001).
[18] G. Karl, S. Meshkov, and J. L. Rosner, Phys. Rev. D **13**, 1203 (1976); P. K. Kabir and A. J. G. Hey, Phys. Rev. D **13**, 3161 (1976).
[19] D. J. Lange, Nucl. Instrum. Methods Phys. Res., Sect. A **462**, 152 (2001); P. Rong-Gang, Chin. Phys. C **32**, 599 (2008).
[20] J. C. Chen, G. S. Huang, X. R. Qi, D. H. Zhang, and Y. S. Zhu, Phys. Rev. D **62**, 034003 (2000).
[21] X. Min *et al.*, Chin. Phys. C **33**, 428 (2009).
[22] B. S. Zou and D. V. Bugg, Eur. Phys. J. A **16**, 537 (2003).
[23] J. M. Link *et al.* (FOCUS Collaboration), Phys. Lett. B **621**, 72 (2005).
[24] M. Ablikim *et al.* (BESIII Collaboration), Phys. Rev. D **87**, 012007 (2013).
[25] M. Ablikim *et al.* (BESIII Collaboration), Phys. Rev. D **83**, 112005 (2011).
[26] M. Ablikim *et al.* (BESIII Collaboration), Phys. Rev. D **87**, 012002 (2013).
[27] N. Berger, K. Zhu, Z. A. Liu, D. P. Jin, H. Xu, W. X. Gong, K. Wang, and G. F. Cao, Chin. Phys. C **34**, 1779 (2010).